ACS Catalysis

RESEARCH ARTICLE

pubs.acs.org/acscatalysis

Aminotroponate/Aminotroponiminate Zinc Complexes Functionalized Mesoporous Silica Catalysts for Intramolecular Hydroamination of Non-Activated Alkenes with Varied Steric and Electronic Properties

Cole Duncan,[§] Ankush V. Biradar,[†,‡] and Tewodros Asefa*[,†,‡]

[†]Department of Chemistry and Chemical Biology, Rutgers, The State University of New Jersey, 610 Taylor Road, Piscataway, New Jersey 08854, United States

[‡]Department of Chemical and Biochemical Engineering, Rutgers, The State University of New Jersey, 98 Brett Road, Piscataway, New Jersey 08854, United States

[§]Department of Chemistry, Syracuse University, 111 College Place, Syracuse, New York 13244, United States

Supporting Information

ABSTRACT: Various aminotroponiminate-/aminotroponate-zinc complexes functionalized mesoporous silica catalysts were synthesized. These included [*N*-propyl-2-(propylamino)troponiminato] zinc methyl (ZnDPRT), [*N*-propyl-2-(phenylamino)troponiminato] zinc methyl (ZnDPHT), and [2-(propylamino) troponato] zinc methyl (ZnPRT) functionalized mesoporous silica catalysts. The catalysts were characterized by various structural (small angle XRD and gas sorption) and compositional (solid-state NMR, XPS, FTIR, and thermogravimetric and elemental analyses) techniques. Their catalytic activities for intramolecular hydroamination of nonactivated alkenes with varied steric and electronic properties were investigated. The catalysts' properties were generally found to differ from one another. This is mainly attributed to (1) fluorosilicate formation during the synthesis of the aminotroponiminate (ATI) ligands on the mesoporous silica, (2) the higher reaction efficiency of the nucleophilic substitution reaction of aminopropyl-functionalized mesoporous silica (API) with tropolone *p*-toluenesulfonate forming 2-(propylamino)troponato- [or aminotroponate (ATO) ligand]-functionalized sample (PRT), compared to that of the ATI ligands, where 2-(alkylamino)tropones or 2-(arylamino)tropones are activated with Et_3OBF_4 forming corresponding vinylgous ethers which then undergo aminolysis with the API precursor, and (3) the different compositional and structural characteristics of the amine/imine (ATI) or amine/carbonyl (ATO) chelation sites. To better understand the catalytic capabilities of the synthesized catalysts, a broader functional group compatibility study was also performed. It was found that decreased bite angles (Thorpe−Ingold effect) and increased electron donation of the *p*-substituted benzylic side arm of the substrates resulted in slightly increased conversion efficiencies in the hydroamination reaction. Overall, the 2,2-diphenyl cyclizing agents formed their corresponding *N*-containing 5-membered heterocycles at 74−94% conversion in 8 h under reflux conditions while the 2,2-dimethyl species exhibited 59−81% conversion of 12 h.

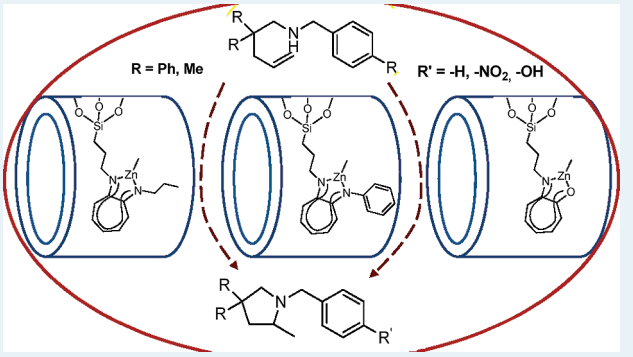

KEYWORDS: intramolecular hydroamination, non-activated alkene, β-aminoalcohol, mesoporous catalyst, aminotroponiminate/aminotroponate-zinc, heterogeneous catalyst

1. INTRODUCTION

The addition of amine across carbon−carbon double or triple bond, also known as hydroamination reaction, is an important chemical transformation which offers an efficient, atom economical route to nitrogen-containing molecules that are useful as fine chemicals for pharmaceuticals, synthetic materials, or chiral building blocks.[1−4] The hydroamination of unsaturated organic compounds to their nitrogen containing analogues or N-containing heterocyclic compounds via intermolecular or intramolecular hydroamination has been reported to be catalyzed by various catalysts including alkali metals,[5] acids,[6] early transition metal (Group IV),[7,8] and late transition metal such as Rh,[9] Pd,[10] and Ni[11,12] complexes.

Zn-complexes have been increasingly considered for hydroamination reactions because of their lesser cost as well as proven

Special Issue: Victor S. Y. Lin Memorial Issue

Received: February 18, 2011
Revised: April 28, 2011
Published: May 05, 2011

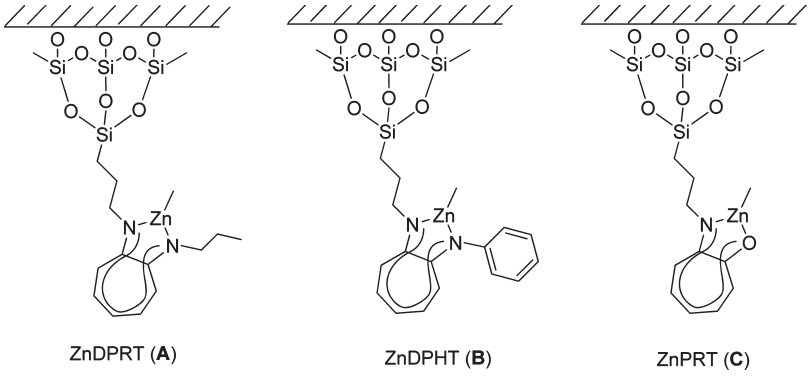

Figure 1. Schematic of mesoporous catalysts [*N*-propyl-2-(propylamino)troponiminato] zinc methyl (ZnDPRT) (**A**), [*N*-propyl-2-(phenylamino) troponiminato] zinc methyl (ZnDPHT) (**B**), and [2-(propylamino)troponato] zinc methyl (ZnPRT) (**C**). (Please note that the binding of the silyl groups is shown via two siloxane bonds for the sake of simplicity; this does not necessarily mean all the ligands were bound to the mesoporous silica surface with two siloxanes; some could be attached via one or two siloxanes).

catalytic activities in hydroamination reactions. Roesky and Blechert, along with their co-workers, have recently published a number of papers related to the synthesis of different types of zinc-aminotroponiminate (Zn-ATI) complexes and their use as homogeneous catalyst for hydroamination reactions.[13−18] By changing the substituents on the aminotroponiminate ligands, they also showed that the catalytic activities of these Zn-complexes can be improved.

Very recently, we have reported the synthesis of the first zinc-aminotroponiminate containing heterogeneous catalyst by tethering 2-(propylamino)troponato] zinc methyl onto mesoporous silica (ZnDPRT) and showed its catalytic activity in the intramolecular hydroamination of 2,2-diphenyl-4-pentenyl)-(4-nitrobenzyl)amine.[19] The material's catalytic activity was found to compete well with homogeneous organometallic catalysts,[20−28] and analogous homogeneous zinc-aminotroponiminate (Zn-ATI) and zinc-aminotroponate (Zn-ATO) catalysts.[14,15,29−32] Furthermore, the catalyst was found to be recyclable up to five times.

However, in our previous study, there were yet unresolved issues related to the ZnDPRT synthesis because of unexpected compositional and structural findings.[19] The elemental analysis data showed a loss of organic (C, H, and N) content when *N*-propyl-2-(propylamino)troponimine (DPRT)-functionalized mesoporous silica was synthesized from the reaction between methyl-capped amine-functionalized mesoporous silica (CAPI) and ethylated 2-(propylamino)tropone. New surface properties shown in the solid-state ^{29}Si NMR, FTIR, TGA, and XPS results, as well as the vibrant yellow color of DPRT, proved ligand formation was successful. Additionally, the formation of Zn−O bonds during complexation of $ZnMe_2$ onto DPRT to form ZnDPRT was observed despite attempts to cap remaining silanols with trimethylsilyl groups, rendering them inert. New observations to be reported here are used to discuss and resolve these discrepancies and shed some more light into the materials chemistry and catalytic activities. Furthermore, our studies here are expanded by the synthesis of two new functionalized SBA-15, Zn-ATI, and Zn-ATO type catalysts, that is, [*N*-propyl-2-(phenylamino)troponiminato] zinc methyl (ZnDPHT) and [2-(propylamino)troponato] zinc methyl (ZnPRT), respectively (Figure 1). The synthesis of the latter materials was accomplished by preparing *N*-propyl-2-(phenylamino) troponiminato (ATI) or 2-(propylamino)troponato (ATO) ligands by sequential coupling reactions onto propylamine-functionalized mesoporous silica (API), and then letting the ligands react with $ZnMe_2$. An example of this synthetic procedure is shown in Figure 2. A broader functional group compatibility study in the hydroamination reaction in the presence of these catalysts has also been performed. To accomplish this, (2,2-diphenyl-4-pentenyl)-(4-nitrobenzyl)amine, (2,2-diphenyl-4-pentenyl)benzylamine, and (2,2-diphenyl-4-pentenyl)-(4-hydroxybenzyl)amine were synthesized for comparison of how electron withdrawal from or donation to the secondary amine affects catalytic efficiency (Scheme 1). To study changes in Thorpe−Ingold effect, (2,2-dimethyl-4-pentenyl)-(4-nitrobenzyl)-amine, (2,2-dimethyl-4-pentenyl)benzylamine, and (2,2-dimethyl-4-pentenyl)-(4-hydroxybenzyl)amine were also synthesized for comparison of how less bulky geminal methyl substituents at the β-position with respect to the amino groups affect the conversion rate of intramolecular hydroamination forming the corresponding nitrogen heterocycles.

In addition, in our previous studies,[19] remaining silanols that were present after 3-aminopropyltrimethoxysilane grafting were capped before the formation of DPRT-functionalized mesoporous material via post modification. The synthesis of the DPRT-functionalized mesoporous material was accomplished by 2-(propylamino)tropone activation with Et_3OBF_4 forming the corresponding vinylgous ether which then will undergo aminolysis with surface aminopropyl groups of the API mesoporous material. Further recent studies,[33] however, proved that Et_3OBF_4 serves as a mild silica etchant and excellent fluorinating agent, resulting in even cleavage of some of the trimethylsilyl capping groups. Because of the observed cleavage of trimethylsilyl capping species upon treatment with the fluorinating agent Et_3OBF_4, the silanol capping step was performed after synthesis of the ATI/ATO ligands in this study. This has provided us further insightful information regarding the best approaches to make Zn-ATI/Zn-ATO type heterogeneous catalysts for hydroamination reactions.

2. EXPERIMENTAL SECTION

Chemicals. Tetraethyl orthosilicate (TEOS), 3-aminopropyltrimethoxysilane (APTMS), propylamine, *N*,*N*-dimethylanilinium tetra(pentafluorophenyl)borate, sodium hydroxide (NaOH), dichloromethane (CH_2Cl_2), $MgSO_4$, hexane, ethyl acetate, and hexamethyldisilazane (HMDS) were all obtained from Sigma-Aldrich and they were used as received without further purification. Anhydrous toluene and ethanol were obtained from Fischer Scientific.

dx.doi.org/10.1021/cs2000945 |*ACS Catal.* 2011, 1, 736–750

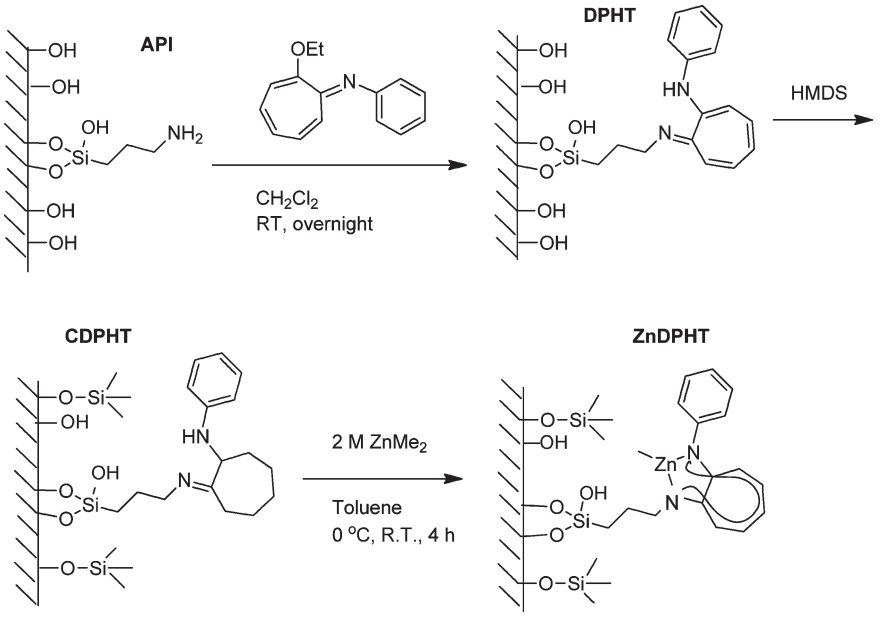

Figure 2. Schematic for the synthesis of mesoporous catalyst, ZnDPHT. The other two catalysts, ZnDPRT and ZnPRT, were also synthesized by following a similar procedure. (Please note that the binding of the silyl groups is shown via two siloxane bonds for the sake of simplicity; this does not necessarily mean all the ligands were bound to the mesoporous silica surface with two siloxanes; some could be attached via one or three siloxanes).

General Methods and Instrumentation. Syntheses were performed under argon atmosphere in dried glassware unless otherwise noted. Reaction solvents were dried with 4 Å, 3.2 mm molecular sieves (Sigma-Aldrich). All other reagents were obtained from commercial sources and used as received. Thin-layer chromatography was performed with silica gel 60 F254 plates (EM Science). Column chromatography was performed with 63−200 mesh, 60 Å silica gel (MP Silitech). Solution ^{1}H and ^{13}C NMR spectra were obtained using a Brüker DPX-300 NMR spectrometer. Solid-state ^{29}Si and ^{13}C CP-MAS spectra were obtained using a 300 MHz Brüker Avance NMR spectrometer. For ^{29}Si CP-MAS NMR experiments, 7.0 kHz spin rate, 10 s recycle delay, 10 ms contact time, $\pi/2$ pulse width of 5.6 μs, and 710−16384 scans using TPPM ^{1}H decoupling were employed. For ^{13}C CP-MAS NMR experiments, 7.0 kHz spin rate, 5 s recycle delay, 1 ms contact time, $\pi/2$ pulse width of 5.2 μs, and 10,000−61,000 scans using TPPM ^{1}H decoupling were employed. Solution ^{1}H- and ^{13}C NMR spectra were obtained using a Brüker DPX-300 NMR spectrometer. FTIR spectra were obtained using a Thermo-Nicolet IR200 spectrometer with samples loaded onto a KBr disk (25 × 4 mm). Thermogravimetric analysis (TGA) or decomposition profiles were acquired for mesoporous materials with a Q500 series thermogravimetric analyzer (TA Instruments). The TGA data were collected under nitrogen atmosphere (60 cm^3/min) in the temperature range of 25−800 °C at a rate of 10 °C/min. Gas adsorption isotherms were obtained using a Micromeritics Tristar 3000 surface area and porosity analyzer. Samples were degassed at 160 °C for 12−16 h and run at 77 K under nitrogen gas adsorption/desorption. The specific surface area (S_{BET}) was calculated according to the Brunauer−Emmett−Teller (BET) method from the adsorption isotherms. Pore size distributions were obtained using the Barrett−Joyner−Halenda (BJH) method from the adsorption branch of the N_2 sorption isotherm. Powder X-ray diffraction (XRD) profiles were obtained using a Scintag powder diffractometer. X-ray photoelectron spectroscopy (XPS) was performed using an XSAM 800 surface analysis system (Kratos) equipped with a Mg Kα X-ray source. A carbon contamination peak with binding energy of 284.8 eV was used as a reference. Elemental analyses of all the materials were carried out by QTI-Intertek (Whitehouse, NJ).

Scheme 1. Intramolecular Hydroamination of Non-Activated Alkenes with Varied Steric and Electronic Properties Catalyzed by Aminotroponiminate (ATI)/Aminotroponate (ATO) Zinc Complexes Functionalized Mesoporous Silica Catalysts

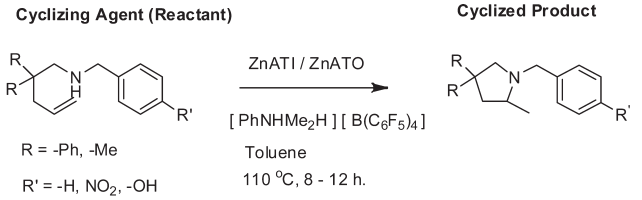

ZnATI = Aminotroponiminate (ATI) Zn complex functionalized mesoporous catalyst
ZnATI = Aminotroponate (ATO) Zn complex functionalized mesoporous catalyst

Synthesis of 2-(Propylamino)tropone. Synthesis was achieved with 62% overall yield as discussed previously[19] with a slightly modified procedure from previous literature.[14,34] Briefly, 2-(tosyloxy)tropone[35] (2.1 g, 7.7 mmol) was dissolved in excess propylamine (15 mL) at 0 °C under stirring. The solution was allowed to stir overnight while warming to room temperature. The reaction was stopped and remaining propylamine was removed under reduced pressure leaving an oily residue. The residue was taken up with 2 M NaOH (15 mL) and CH_2Cl_2 (30 mL) and extracted (CH_2Cl_2, 2 × 30 mL). The combined organic extracts were washed with brine, dried with $MgSO_4$, and purified by column chromatography (7:1 hexane: EtOAc) to give 1.1 g of the oily brown residue *N*-(propylamino) tropone (88%).

dx.doi.org/10.1021/cs2000945 |*ACS Catal.* 2011, 1, 736–750

^{1}H NMR ($CDCl_3$, 300 MHz): δ 1.04 (t, $-CH_2CH_2CH_3$, J = 12.2 Hz, 3H), 1.79 (sextet, $-CH_2CH_2CH_3$, J = 7.2 Hz, 2H), 3.29 (q, $-CH_2CH_2CH_3$, J = 6.6 Hz, 2H), 6.54 (d, J = 10.2 Hz, 1H), 6.67 (t, J = 9.3 Hz, 1H), and 7.13−7.30 (m, 3H) ppm. ^{13}C NMR ($CDCl_3$, 300 MHz): δ 12.09 (C_{10}), 22.19 (C_9), 45.04 (C_8), 109.00 (C_6), 122.37 (C_2), 128.76 (C_4), 136.69 (C_5), 137.65 (C_3), 156.11 (C_1−N), and 177.02 (C_7=O) ppm.

Synthesis of 2-(Phenylamino)tropone. Synthesis was performed according to previously reported literature.[36] 2-(Tosyloxy)tropone (1.60 g, 5.8 mmol) was dissolved in EtOH (30 mL) and refluxed with aniline (0.56 mL, 6.1 mmol) for 24 h. The solvent was evaporated, and the crude was purified by column chromatography (4:1 hexane:EtOAc) to afford an oily brown residue (609 mg, 54%). ^{1}H NMR ($CDCl_3$, 300 MHz): δ 6.79 (tdd, J = 12.2 Hz, 3H), 7.11−7.19 (m, 2H) (sextet, $-CH_2CH_2CH_3$, J = 7.2 Hz, 2H), 7.21−7.39 (m, 5H), 7.45 (m, 2H), and 8.78 (br. s, 1H) ppm. ^{13}C NMR ($CDCl_3$, 300 MHz): δ 110.9, 124.6, 125.0, 126.4, 130.1, 131.0, 136.4, 137.9, 138.7, 154.1, and 177.4 ppm.

Synthesis of (2,2-Diphenyl-4-pentenyl)benzylamine. Synthesis was performed according to previously reported literature.[21] ^{1}H NMR ($CDCl_3$, 300 MHz): δ 0.91 (br s, 1H), 3.09 (d, J = 6.9 Hz), 3.25 (s, 2H), 4.92−5.06 (m, 2H), 5.37 (tdd, J = 6.9, 10.2, 17.1 Hz, 1H), 3.76 (s, 2H), and 7.19−7.30 (m, 16H) ppm. ^{13}C NMR ($CDCl_3$, 300 MHz): δ 41.4, 50.1, 54.1, 55.2, 117.5, 125.9, 126.1, 126.6, 127.7, 127.8, 127.9, 128.0, 128.1, 134.8, 140.7, and 146.8 ppm.

Synthesis of (2,2-Diphenyl-4-pentenyl)-(4-hydroxybenzyl)amine. Synthesis was performed according to previously reported literature.[21] ^{1}H NMR ($CDCl_3$, 300 MHz): δ 3.03 (d, J = 6.9 Hz), 3.03 (d, J = 6.9 Hz), 3.17 (s, 2H), 3.63 (s, 2H), 4.89−5.03 (m, 2H), 5.33 (m, 1H), 6.69 (d, 8.7 Hz, 2H), 7.00 (d, 12 Hz, 2H), and 7.04−7.29 (m, 12H) ppm. ^{13}C NMR ($CDCl_3$, 300 MHz): δ 41.5, 50.0, 53.5, 55.0, 115.0, 17.6, 125.9, 127.9, 129.2, 134.7, and 146.6 ppm.

Synthesis of (2,2-Dimethyl-4-pentenyl)benzylamine. Synthesis was performed according to previously reported literature.[21] ^{1}H NMR ($CDCl_3$, 300 MHz): δ 1.00 (s, 6H), 1.25 (br. s, 1H), 2.12 (dd, J = 7.5, 8.4 Hz, 1H), 2.46 (s, 2H), 3.87 (s, 2H), 5.08−5.27 (m, 2H), 5.90 (m, 1H), and 7.32−7.40 (m, 5H) ppm. ^{13}C NMR ($CDCl_3$, 300 MHz): δ 26.1, 34.9, 45.2, 60.2, 117.3, 127.3, 128.5, 128.8, 136.1, and 141.6 ppm.

Synthesis of (2,2-Dimethyl-4-pentenyl)-(4-hydroxybenzyl)amine. Synthesis was performed according to previously reported literature.[21] ^{1}H NMR ($CDCl_3$, 300 MHz): δ 0.87 (s, 6H) 2.01 (d, J = 7.5 Hz, 1H), 2.38 (s, 2H), 4.98−5.03 (m, 2H), 5.71−5.88 (m, 1H), 6.70 (d, J = 8.4 Hz, 2H), 7.13 (d, J = 8.4 Hz, 2H). ^{13}C NMR ($CDCl_3$, 300 MHz): δ 26.0, 34.6, 45.2, 54.7, 60.1, 116.1, 117.5, 130.0, and 135.6 ppm.

Synthesis of (2,2-Dimethyl-4-pentenyl)-(4-nitrobenzyl)amine. Synthesis was performed according to previously reported literature.[21] ^{1}H NMR ($CDCl_3$, 300 MHz): δ 0.88 (s, 6H), 1.31 (br. s, 1H), 2.00−2.03 (m, 2H), 2.33 (s, 2H), 3.88 (s, 2H), 4.97−5.02 (m, 2H), 5.70−5.85 (m, 1H), 7.50 (d, J = 8.7 Hz, 2H), 8.15 (d, J = 8.7 Hz, 2H) ppm. ^{13}C NMR ($CDCl_3$, 300 MHz): δ 25.8, 34.7, 45.0, 54.2, 60.0, 117.3, 123.8, 128.8, 128.9, 135.8, 147.2, and 149.4 ppm.

Synthesis of *N*-Propyl-2-(propylamino)troponimine Functionalized Mesoporous Material (DPRT). The synthesis of the catalysts was achieved following the procedure shown in Figure 2. First 3-aminopropyl-functionalized SBA-15 (API) was synthesized by stirring 3-aminopropyltrimethoxysilane (APTMS) in solution of calcined SBA-15 dispersed in isopropanol as performed previously.[19] A reaction mixture containing ethylated *N*-(propylamino)tropone was prepared by adding 1 M EtO_3BF_4 (2.50 mL, 2.50 mmol) in CH_2Cl_2 dropwise into a solution *N*-(propylamino)tropone (0.41 g, 2.50 mmol) in CH_2Cl_2 (8 mL) and stirring the solution for 3 h. This reaction mixture was then mixed with API (1.0 g) in CH_2Cl_2 (100 mL) and stirred at room temperature for 16 h forming a yellow *N*-propyl-2-(propylamino)troponimine functionalized mesoporous silica powder, labeled as DPRT. Remaining silanol groups were then capped by stirring DPRT (0.8 g) in toluene (50 mL) with excess hexamethyldisilazane (HMDS) (5 mL) at room temperature for 24 h to form methyl-capped DPRT (or CDPRT). The resulting yellow mesoporous powder (CDPRT) was recovered by vacuum filtration and washed copiously with ethanol (95%). The material was dried overnight at 85 °C and stored in a desiccator for future use. The same procedure was utilized to produce DPHT/CDPHT (Figure 2).

Synthesis of *N*-(Propylamino)tropone Functionalized Mesoporous Material (PRT). API (1.0 g) was dispersed in EtOH (95%, 100 mL) via sonication. 2-(Tosyloxy)tropone[35] (0.56 g) was then added to the API solution. The resulting mixture was then stirred for 16 h under reflux. The resulting yellow-green product, *N*-(propylamino)tropone functionalized mesoporous silica (PRT), was then separated via vacuum filtration and washed with CH_2Cl_2 (500 mL), dried overnight at 85 °C, and stored in a desiccator until further use. Capping of PRT with methyl groups using HMDS was performed as with CDPRT/CDPHT, yielding a light yellow mesoporous powder (CPRT).

Synthesis of [*N*-Propyl-2(propylamino)troponiminato] Zinc Methyl Functionalized Mesoporous Catalyst (ZnDPRT). A solution of 0.5 g of DPRT in dry toluene (100 mL) was prepared via sonication. Then 0.5 mL of 2 M $ZnMe_2$ (1.0 mmol in toluene) was added dropwise to the reaction vessel and allowed to stir at room temperature for 6 h. The resulting yellow powder (ZnDPRT catalyst) was recovered by vacuum filtration and washed with 500 mL of ethanol (95%). The material was dried overnight at 85 °C and stored in a desiccator for future use. The same procedure was utilized to produce ZnDPHT and ZnPRT catalysts.

Intramolecular Hydroamination Catalysis. Experiments were performed as in previously published studies.[19] In a typical cyclization experiment, ZnDPRT (20 mg) was suspended via sonication in 5 mL of toluene followed by addition of cyclizing agent (0.15 mmol) and *N,N*-dimethylanilinium tetra(pentafluorophenyl)borate (20 mg, 0.024 mmol). The reaction mixture was heated to 120 °C and stirred until completion. Products were isolated via column chromatography. Their yields were determined via gas chromatography (GC) and ^{1}H NMR spectroscopy. The ^{1}H NMR results are included below.

Intramolecular Hydroamination Catalysis Products. *2-Methyl-1-benzyl-4,4-diphenylpyrrolidine.* ^{1}H NMR ($CDCl_3$, 300 MHz): δ 1.20 (d, J = 6 Hz, 3H), 2.21−2.28 (m, 1H), 2.80−2.99 (m, 3H), 3.29 (d, 13.2 Hz, 1H), 3.68 (d, J = 9.9 Hz, 1H), 4.13 (d, J = 13.2 Hz 1H), and 7.12−7.42 (m, 15H) ppm. ^{13}C NMR ($CDCl_3$, 300 MHz): δ 19.9, 30.2, 48.4, 53.0, 55.8, 58.5, 60.1, 66.9, 125.9, 126.3, 127.2, 127.7, 127.9, 128.1, 128.3, 128.6, 128.7, 129.1, 140.5, 149.1, and 151.0 ppm.

1-(4-Hydroxybenzyl)-2-methyl-4,4-diphenylpyrrolidine. ^{1}H NMR ($CDCl_3$, 300 MHz): δ 1.20 (d, J = 6 Hz, 3H), 2.24−2.29 (m, 1H), 2.85−2.95 (m, 3H), 3.22 (d, 12.9 Hz, 1H), 3.64−3.69 (m, 1H),

dx.doi.org/10.1021/cs2000945 |*ACS Catal.* 2011, 1, 736–750

4.02 (d, J = 12.9 Hz 1H), 6.73−6.80 (m, 2H), and 7.10−7.30 (m, 12H) ppm. ^{13}C NMR ($CDCl_3$, 300 MHz): δ 19.2, 30.9, 45.2, 47.8, 52.4, 57.3, 59.5, 66.0, 115.1, 125.4, 125.7, 127.1, 127.3, 127.8, 128.1, 131.2, 148.6, 150.2, and 154.7 ppm.

1-Benzyl-2-methyl-4,4-dimethylpyrrolidine. ^{1}H NMR ($CDCl_3$, 300 MHz): δ 0.98 (s, 3H), 1.08 (s, 3H), 1.15 (d, J = 6 Hz, 3H), 1.32 (dd, J = 9, 12.3, 21.3 Hz, 1H), 1.60−1.76 (m, 1H), 1.94 (d, J = 9 Hz, 1H), 2.50−2.60 (m, 1H), 2.65 (d, J = 9.3 Hz, 1H), 3.11 (d, J = 13.2 Hz, 1H), 4.10 (d, J = 13.2 Hz, 1H), and 7.22−7.34 (m, 5H) ppm. ^{13}C NMR ($CDCl_3$, 300 MHz): δ 19.9, 29.6, 31.0, 35.8, 49.5, 58.4, 60.2, 68.8, 127.0, 128.5, and 129.1 ppm.

2-Methyl-1-(4-hydroxybenzyl)-4,4-dimethylpyrrolidine. Because of decomposition of this product during catalyst and column chromatography, data was obtained from crude mixture of starting reagent and product. ^{1}H NMR ($CDCl_3$, 300 MHz): δ 1.03 (s, 3H), 1.08 (s, 3H), 1.26 (d, J = 6.3 Hz, 3H), 1.46 (dd, J = 10.2, 12.9, 23.1 Hz, 1H), 1.81−1.88 (m, 1H), 1.96−2.04 (m, 1H), 2.50−2.60 (m, 1H), 2.44 (d, J = 10.2 Hz, 1H), 3.23 (d, J = 12.9 Hz, 1H), 4.00 (d, J = 13.2 Hz, 1H), 6.64 (d, J = 8.4 Hz, 2H), 6.68−6.74 (m, 2H), and 6.96−7.20 (m, 5H) ppm. ^{13}C NMR ($CDCl_3$, 300 MHz): δ 18.2, 24.9, 29.6, 30.0, 35.1, 36.0, 40.4, 41.3, 44.4, 48.6, 52.5, 58.0, 61.5, 67.7, 113.6, 115.8, 116.5, 117.9, 125.7, 128.6, 129.4, 129.8, 130.3, 130.4, 130.5, and 131.4 ppm.

2-Methyl-1-(4-nitrobenzyl)-4,4-dimethylpyrrolidine. ^{1}H NMR ($CDCl_3$, 300 MHz): δ 0.99 (s, 3H), 1.09 (s, 3H), 1.13 (d, J = 6 Hz, 3H), 1.32 (dd, J = 8.7, 12.3, 21 Hz, 1H), 1.72−1.79 (m, 1H), 1.92 (d, 8.7 Hz, 1H), 2.57−2.62 (m, 2H), 3.21 (d, J = 14.4, 1H), 4.04 (d, J = 14.4 Hz, 1H), 7.50 (d, J = 8.4 Hz, 2H), and 8.15 (d, J = 8.7 Hz, 2H) ppm. ^{13}C NMR ($CDCl_3$, 300 MHz): δ 20.0, 29.4, 31.0, 36.1, 49.3, 57.8, 60.4, 69.0, 123.8, 129.4, and 149.0 ppm.

3. RESULTS AND DISCUSSION

Synthesis. Three different aminotroponiminate (ATI) or aminotroponate (ATO) zinc methyl complexes functionalized mesoporous silica heterogeneous catalysts were synthesized for intramolecular hydroamination of nonactivated alkenes with varied steric and electronic properties. By varying the catalysts and the substrates, we investigated the properties related to bite angles (Thorpe−Ingold effect) and electron donation of the *p*-substituted benzylic side arm of the substrates with respect to catalytic activities. The catalysts included [*N*-propyl-2-(propylamino) troponiminato] zinc methyl (ZnDPRT), [*N*-propyl-2-(phenylamino)troponiminato] zinc methyl (ZnDPHT), and [2-(propylamino)troponato] zinc methyl (ZnPRT) functionalized mesoporous silica catalysts (Figure 1). They were synthesized by preparing *N*-propyl-2-(propylamino)troponiminato, *N*-propyl-2-(phenylamino)troponiminato or 2-(propylamino)troponato ligands onto 3-aminopropyl functionalized mesoporous silica (API), and then letting $ZnMe_2$ react with the ligands, as shown in Figure 2. The structures and compositions of catalysts as well as their catalytic activities in the intramolecular hydroamination reaction of a series of reactants were then studied.

Structural Analyses. N_2 gas sorption studies were performed to monitor the changes in surface area, pore size distribution, and pore volume at all stages of catalyst preparation. The isotherms and their corresponding BJH pore size distributions (PSDs) for ZnDPRT, ZnDPHT, and ZnPRT, as well as their precursors, are shown in Figure 3. The structural data for all steps in the synthesis each catalyst is displayed in Table 1.

The parent SBA-15 (not shown) had a BET surface area of 841 m^2/g, an average pore diameter of 6.2 nm, and an average pore volume of 0.90 cm^3/g. Upon APTMS grafting and forming API, the surface area and pore volume showed significant decrease to 499 m^2/g and 0.64 cm^3/g, respectively, while the average pore diameter showed only minor reduction (6.2 Å). The nitrogen sorption isotherm shows a type IV isotherm with sharp capillary condensation from P/P_o = 0.60 to 0.75, indicating the presence of uniform mesopores in the materials. The use of Et_3OBF_4 as an ethylating agent toward imine formation with surface aminopropyl groups for the synthesis of DPRT and DPHT has, as discussed in our previous report,[33] also been found to cause fluorination and mild etching of the silica surface because of the nucleophilic substitution of F^- (from the equilibrium reaction of $BF_4^- \leftrightarrow BF_3 + F^-$) with surface silanols or cleavage of Si−O−Si bonds within the fully condensed mesostructure.[33] Pore diameter increases to 7.2 and 6.7 nm for DPRT and DPHT, respectively, with concomitant reduction of surface area to 320 and 368 m^2/g were observed. The nitrogen sorption isotherms for both samples shift toward larger P/P_o. After capping and $ZnMe_2$ addition the average pore diameter is decreased to 6.2 nm (ZnDPRT) and 6.1 nm (ZnDPHT). The nitrogen sorption isotherms of both samples exhibit a much broader P/P_o range of ∼0.42−0.75 and slight volume reductions, indications that $ZnMe_2$ addition causes some pore constriction or bottlenecking. It may be noticed, however, that the surface areas of ZnDPRT and ZnDPHT both exhibit slightly increased surface areas (358 and 371 m^2/g) which may be due to the loss of unreacted/physisorbed 2-alkylaminotropone that was not successfully removed via EtOH washings after DPRT and DPHT syntheses, but was after the capping step where the catalyst is stirred in toluene for 24 h. Reaction of API with tropolone *p*-toluenesulfonate yielded PRT, which had the highest surface area (436 m^2/g) and lowest pore diameter (6.0 nm) of all catalyst precursors. The final catalyst (ZnPRT) exhibited a similar nitrogen sorption isotherm and surface area as the former catalysts; however, the average pore diameter and volume were noticeably lower because of a higher loading efficiency of the PRT ligand synthesis compared to that of the ATI ligands, as will be shown in elemental analysis data below.

Figure 4 displays the small angle XRD patterns for the Zn aminotroponiminate (Zn-ATI) and Zn aminotroponato (Zn-ATO) catalysts and their respective precursors. The parent SBA-15 material exhibits a well-defined (100) Bragg reflection as well as discernible (110) and (200) Bragg reflections at 2θ = 1.00°, 1.66°, and 1.84°, respectively. After grafting with aminopropyl groups, these Bragg reflections shift to 0.96°, 1.60°, and 1.82°, respectively, indicating slightly higher lattice spacing. It can be seen that the DPRT and DPHT and their trimethylsilyl-capped counterparts show better defined (110) and (200) reflections than those of the parent materials (or SBA-15 and API) because of advantageous pore reconstruction due to the surface fluorination, whereas PRT does not display the same tendency. These findings are in good agreement with surface fluorination studies performed on the sulfonic acid functionalized SBA-15 catalyst presented in ref 33. After zinc addition, however, these Bragg reflections are slightly diminished in all three materials. This may be due to the presence of zinc-complex agglomerates which decrease the contrast or constructive X-ray scattering effects between the channels pores and the channel wall, broadening the peaks.

The X-ray diffraction (XRD) patterns for the three samples, that is, ZnDPRT, ZnDPHT, and ZnPRT, were somewhat similar. The maximum of the most intensive diffraction line was barely changed indicating that the well-ordered mesostructure in the materials remained intact and unchanged after each step of

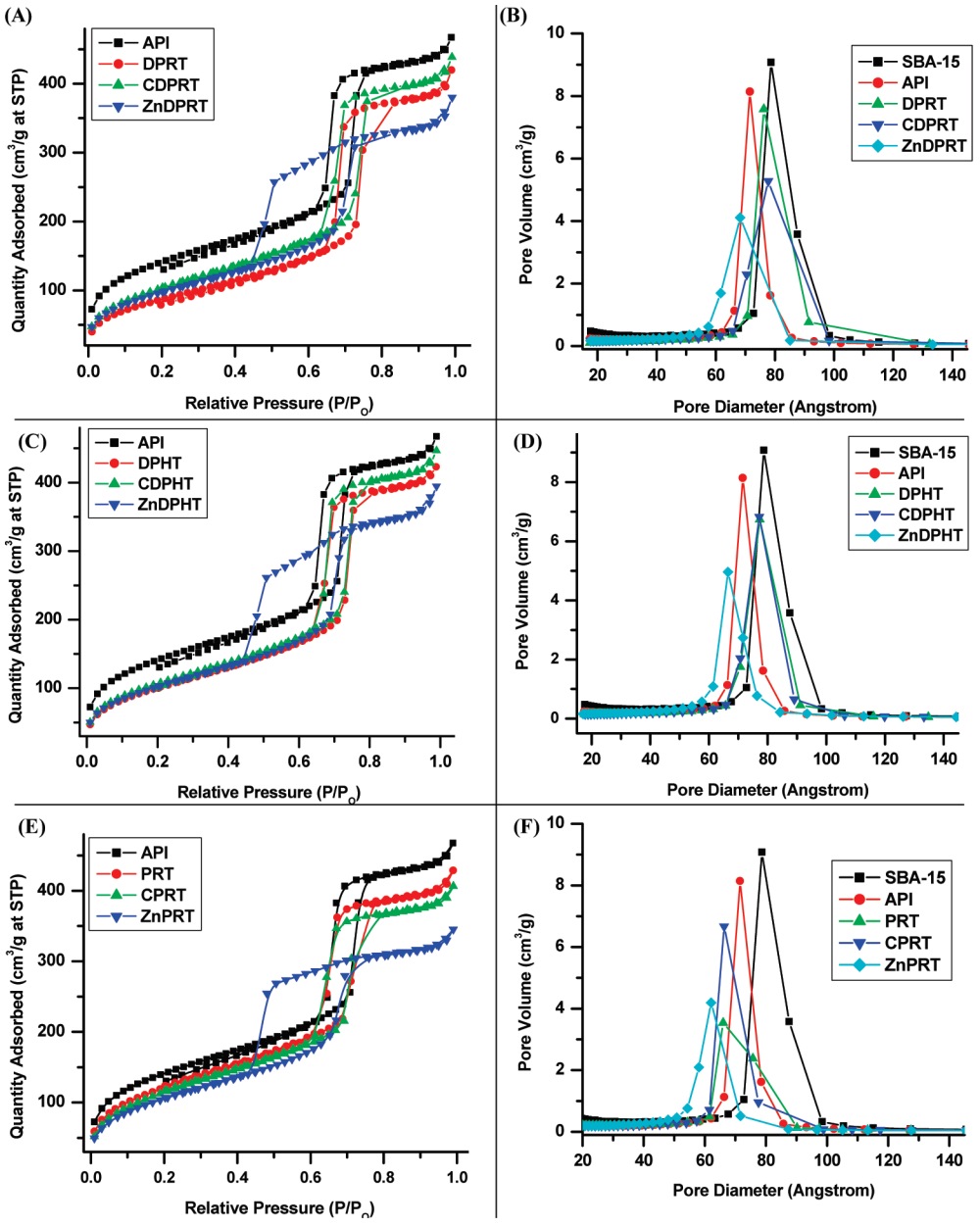

Figure 3. (A) N_2 gas sorption isotherms and (B) BJH pore size distribution for ZnDPRT and precursors thereof. (C) N_2 gas sorption isotherms and (D) BJH pore size distribution for ZnDPHT and precursors thereof. (E) N_2 gas sorption isotherms and (F) BJH pore size distribution for ZnPRT and precursors thereof. The BJH pore size distributions were obtained from the adsorption branch of the N_2 gas adsorption isotherms.

materials synthesis. It is known that the XRD patterns provide information regarding the lattice spacing of the materials or the center-to-center distance between the channels. Thus, the result indicates that the lattice spacings of these mesostructured materials (catalysts) were similar to one another, or they barely changed after the different surface modification reactions.

On the other hand, unlike the XRD patterns, the N_2 gas isotherms of the materials changed after the surface modification reactions. Furthermore, they changed differently for the different samples. Please note that pore diameters of mesoporous materials can change without affecting lattice spacings (or XRD patterns). In Figure 3, it can be noticed that the saturation pore volume of ZnPRT was smaller than those for samples ZnDPRT and ZnDPHT. This may be because (1) the organic ligands/complexes in the former were bulkier than those in the latter, (2) the surface modification caused the walls of the latter to enlarge because of surface etching, or (3) both. Because the sizes of the ligands/complexes in the three materials were somewhat similar, or actually slightly smaller in the case of ZnPRT compared to ZnDRT and ZnDPHT, the differences in N_2 gas isotherms were more likely to do with the latter. This conclusion makes sense considering the fact that EtO_3BF_4 was reported to etch the walls and enlarge the pores of mesoporous silica,[33] and that EtO_3BF_4 was used only in the synthesis of ZnDPRT and ZnDPHT materials, in which higher pore volume was observed (Table 1).

Compositional Analyses. To aid in elucidation of the structural differences shown by nitrogen gas sorption and small angle

dx.doi.org/10.1021/cs2000945 |*ACS Catal.* 2011, 1, 736–750

Table 1. Structural Data for Zn-ATI and Zn-ATO Catalysts and Their Precursors

sample	unit cell (nm)[a]	average pore diameter (nm)[b]	BET surface area (m^2/g)	BJH average pore volume (cm^3/g)[b]
SBA-15	10.2	6.2	841	0.90
API	10.6	6.2	499	0.64
DPRT	11.3	7.2	320	0.61
CDPRT	11.7	6.7	380	0.62
ZnDPRT	12.1	6.2	358	0.54
DPHT	11.6	6.7	368	0.60
CDPHT	11.7	6.8	388	0.63
ZnDPHT	12.4	6.1	371	0.56
PRT	12.4	6.0	436	0.59
CPRT	11.3	6.0	419	0.56
ZnPRT	11.9	5.4	385	0.47

[a] $a_o = 2d_{100}/3^{1/2}$ ($\times 10^{-1}$ nm) for 2-D hexagonally ordered materials. [b] Obtained from adsorption branch of the N_2 gas sorption isotherms.

XRD studies, thermogravimetric and elemental analyses were carried out. Spectroscopic methods were also performed including solid state ^{13}C and ^{29}Si CP-MAS NMR spectroscopy, FTIR spectroscopy, and XPS spectroscopy.

The solid-state ^{29}Si and ^{13}C CP-MAS spectra for ZnDPRT and its precursors are displayed in Figure 5. As shown in the ^{29}Si spectra, API (also shown in Figures 6 and 7) has peaks at −112 and −103 ppm from Q^4 and Q^3 silicate species and T^3 silicates at −69 ppm corresponding to $(SiO)_3Si$-$(CH_2)_3$-NH_2 and a shoulder at −61 ppm which corresponds to $(SiO)_2$ $SiOH$-$(CH_2)_3$-NH_2, or T^2 silicate species. The ^{13}C spectrum of API shows five main peaks. Peaks corresponding to the propyl carbons can be seen at 9 ppm (Si−CH_2−CH_2−CH_2−NH_2), 24 ppm (Si−CH_2−CH_2−CH_2−NH_2), and 44 ppm (Si−CH_2−CH_2−CH_2−NH_2).[37−40] The peaks shown at 59 and 67 ppm are the result of ethoxy and isopropxy species, which form when surface silanols and alcohols used as solvents undergo reaction.[37] Upon formation of DPRT (Figure 5 B, left), the Q^3 peaks are fluorinated, as shown in ref 19, and a major Q^4 peak centered at −112 ppm and only a weaker shoulder corresponding to Q^3 peak are observed. It is also shown that the shoulders at −62 and −60 ppm disappear leaving one T peak centered around −68 ppm. The ^{13}C spectrum of DPRT (Figure 5 B, right) shows the formation of a broad set of peaks from 100−160 ppm corresponding to the tropone ring carbons. The propyl carbon at 44 ppm shifts downfield slightly and the peak previously at 24 ppm shifts upfield to 21 ppm. It is also noticed that the peaks at 59 and 67 ppm are almost completely removed because of fluorination via nucleophilic substitution by EtO_3BF_4. The chelation of zinc to the DPRT, forming ZnDPRT (Figure 5 C, right) is evidenced by the slight change of relative peak intensities in the 100−160 ppm range while the propyl peaks, now centered at 10, 22, and 44 ppm, see only minor shifts.

The solid-state ^{29}Si and ^{13}C CP-MAS spectra for ZnDPHT and its precursors are shown in Figure 6. The ^{29}Si spectrum of DPHT (Figure 6 B, left) shows results similar to that of DPRT, as expected, due to similar post modification methodologies.

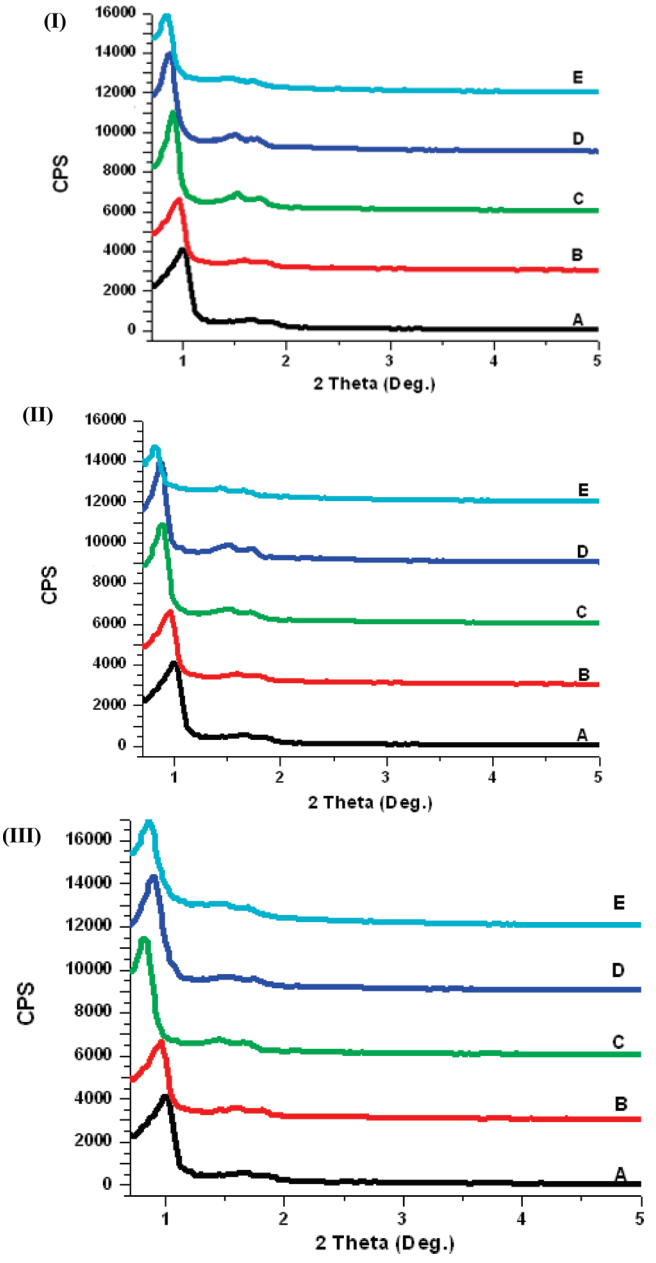

Figure 4. (I) XRD patterns of ZnDPRT series: (A) SBA-15, (B) API, (C) DPRT, (D) CDPRT, and (E) ZnDPRT. (II) XRD patterns of ZnDPHT series: (A) SBA-15, (B) API, (C) DPHT, (D) CDPHT, and (E) ZnDPHT. (III) XRD patterns of ZnPRT series: (A) SBA-15, (B) API, (C) PRT, (D) CPRT, and (E) ZnPRT.

The ^{13}C spectrum of DPHT (Figure 6 B, right) shows a broad set of new peaks from 100−160 ppm with clearly visible peaks at 105, 120 (shoulder), 129, 141, 153, and 160 ppm. These broad set of new peaks from 100−160 ppm can be attributed to the different carbon atoms of the 2-(phenylamino)troponiminato moiety of the DPHT ligand. The propyl peaks are seen at 9, 21, and 44 ppm, respectively, as seen with DPRT, and the peaks at 59 and 67 ppm are also significantly diminished because of fluorination via nucleophilic substitution. The formation ZnDPHT (Figure 6 C, right) is evidenced by the slight changes exhibited in the 100−160 ppm range. The peaks previously shown at 105, 153, and 160 ppm are broadened, and the shoulder

dx.doi.org/10.1021/cs2000945 |ACS Catal. 2011, 1, 736–750

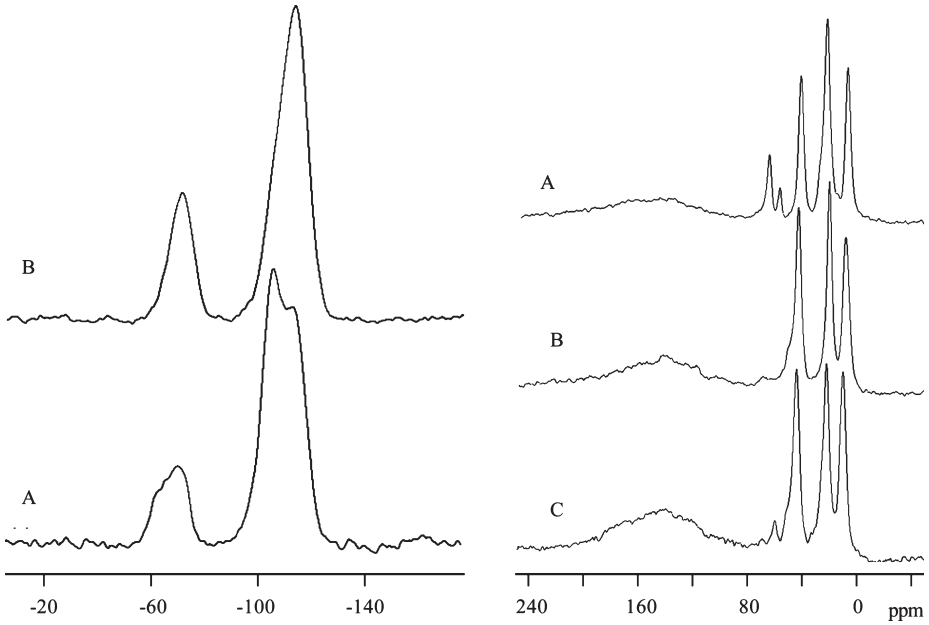

Figure 5. ^{29}Si (left panel) and ^{13}C (right panel) CP-MAS NMR spectra for (A) API and (B) DPRT and (C) ZnDPRT.

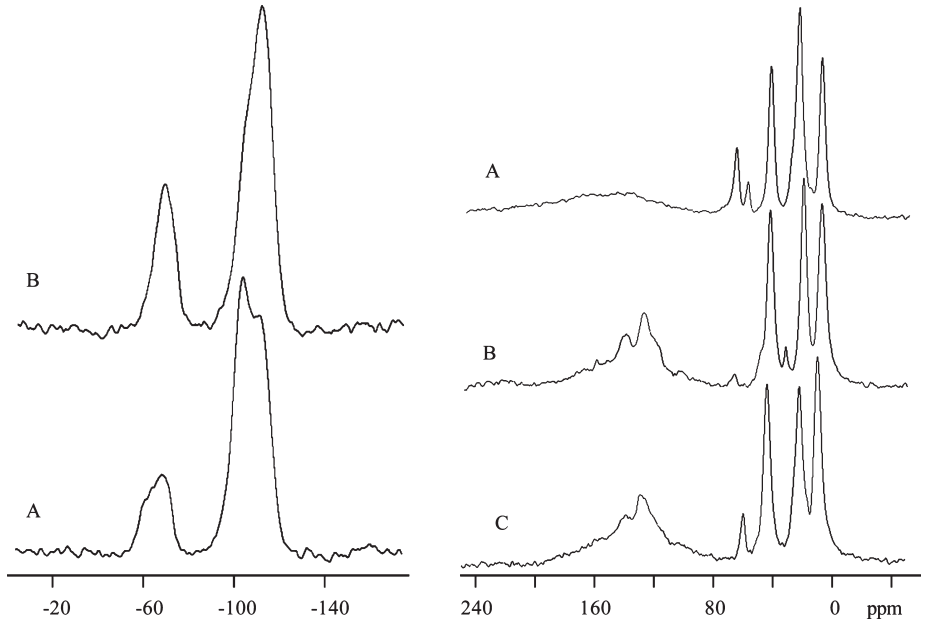

Figure 6. ^{29}Si (left panel) and ^{13}C (right panel) CP-MAS NMR spectra for (A) API and (B) DPHT and (C) ZnDPHT.

at 120 ppm is not very visible. Deformation and broadening of the major peaks seen at 129 and 141 ppm are also shown to occur. It is also noticed that a new peak at 60 ppm corresponding to ethoxy carbon appears.

The solid-state ^{29}Si and ^{13}C CP-MAS spectra for ZnPRT and its precursors are displayed in Figure 7. The ^{29}Si spectrum of PRT (Figure 7 B, left) does not show the removal of Q^3, or the smoothing of the T peaks, as shown with the ATI samples. As shown with the ATI samples, the ^{13}C CP-MAS spectrum of PRT shows a broad set of new peaks from 90−180 ppm with major peaks at 129 and 138 ppm as well a multiple minor, but distinguishable, peaks in the range of 150−180 ppm. The propyl peaks are seen at 9, 22, and 43 ppm, respectively. The ethoxy and isopropxy peaks at 59 and 67 ppm are still clearly visible, unlike the ATI samples, because EtO_3BF_4 is not used in the synthetic protocol. The formation ZnPRT is evidenced by marked changes the relative intensities of the peaks at 129 and 138 ppm as well as the other minor peaks in the region.

Supporting Information, Figures S1−S4 display the TGA profiles for the Zn-ATI and Zn-ATO catalysts and are shown in conjunction with their precursors. The wt % loss from 100−600 °C, the region where organic species and surface silanols are removed, for all catalysts and their precursors are compared in Table 2. As shown with the structural analysis, the ATI samples, synthesized via post modification using EtO_3BF_4, show similar trends whereas PRT has a distinct profile

dx.doi.org/10.1021/cs2000945 |*ACS Catal.* 2011, 1, 736–750

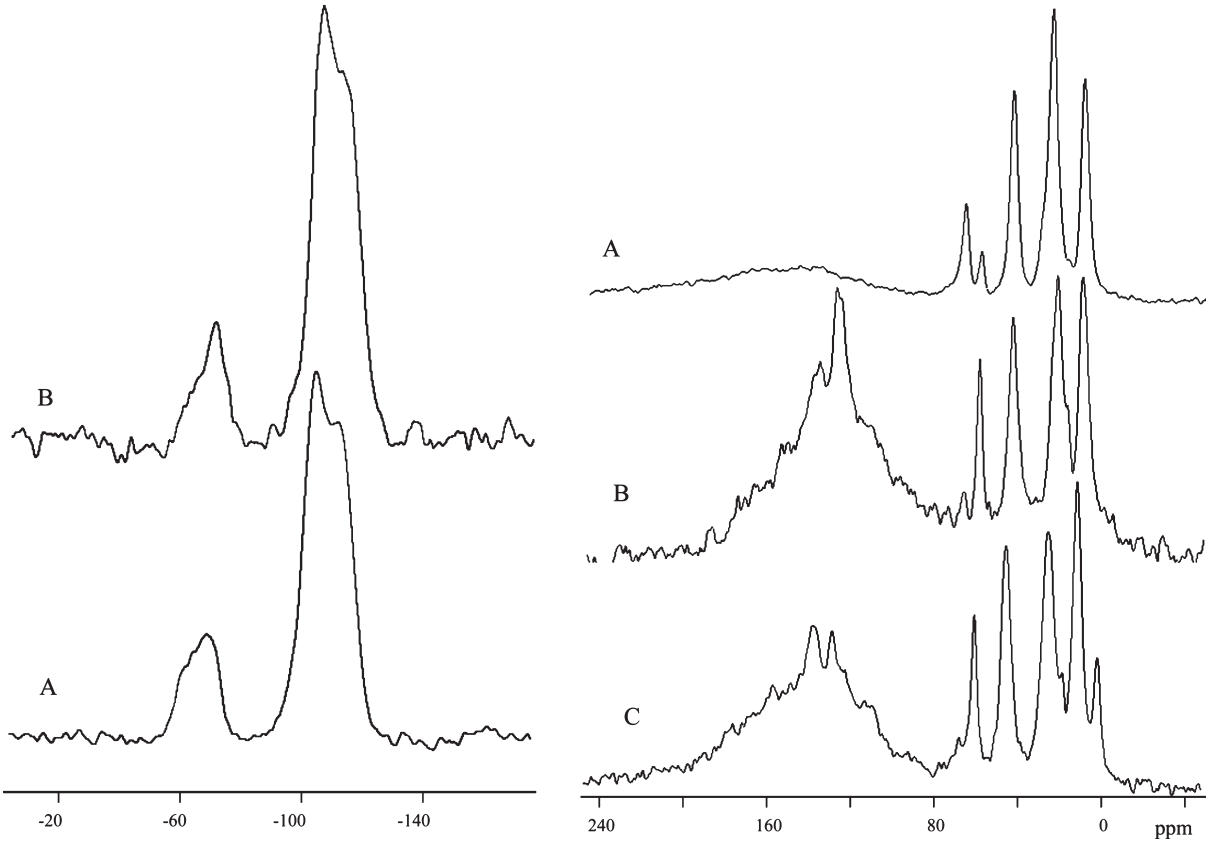

Figure 7. ^{29}Si (left) and ^{13}C (right) CP-MAS NMR spectra for (A) API and (B) PRT and (C) ZnPRT.

(Supporting Information, Figure S4). The starting mesoporous material API shows three distinct regions of wt % loss: (1) 25−100 °C (physisorbed H_2O), (2) 100−300 °C, and (3) 300−600 °C. The two higher temperature regions are likely a combination of the condensation of geminal or H-bonded silanols and aminopropyl species followed by the loss of isolated surface silanols at temperatures >400 °C, as reported in ref 33. DPRT and DPHT show significant weight loss from 200−350 °C corresponding to the loss of the ATI ligands, in agreement with previous findings.[19] Unlike the ATI mesoporous materials, PRT shows a smoother wt % loss over the same region, possibly because of the lower molecular weight of the covalently attached ligand. Additionally the fluorination process, which occurs during synthesis of the ATI ligands, replaces surface silanols with fluorosilicate species. This makes the silanol groups not to contribute as much to weight losses on the TGA profiles of the ATI samples. On the other hand, silanols remain present after the synthesis of PRT and contribute to the wt % loss over the entire region, albeit not significantly. It is worth nothing that the loss of silanols occurs over large temperature ranges compared to the loss of organic and fluoro groups over narrow temperature ranges of ≈200−400 °C. In addition, as shown in the TGA profiles, the region of wt % loss corresponding to ATI ligands was also altered after capping with HMDS.

During experimentation, it was noticed that, upon completion of the capping process and copious washing with ethanol, the resulting eluate was slightly yellow because of the removal of physisorbed ATI/ATO species that had not been removed during the initial washing step. It should be noted, however, that after this step and zinc chelation, the catalysts remained vibrantly yellow and retained much of the ATI/ATO functionality, as proven by ^{29}Si and ^{13}C CP-MAS NMR as well as FTIR and XPS studies to be discussed later. Upon zinc addition, all three catalysts exhibit a lower wt % loss in the organic region, as expected, because of the formation of highly thermally stable ZnO which contributes to the overall wt % of the materials, lowering the relative wt % of organic components within the mesoporous silica.

Table 2. Weight Loss (%) Occurring in the 100−600 °C Region

sample	wt % changes in the range 100−600 °C
SBA-15	3.8
API	12.3
DPRT Samples	
DPRT	15.2
CDPRT	13.1
ZnDPRT	12.2
DPHT Samples	
DPHT	14.2
CDPHT	10.7
ZnDPHT	10.5
PRT Samples	
PRT	12.9
CPRT	11.7
ZnPRT	10.1

dx.doi.org/10.1021/cs2000945 |*ACS Catal.* 2011, 1, 736–750

Table 3. Chemical Compositions of ZnATI/ATO Catalysts and Their Precursors

	chemical composition (wt %)				
sample	C	H	N	F	Zn
CAPI[a]	8.9	2.3	2.2		
DPRT[a]	7.1	1.7	2.1		
ZnDPRT[a]	5.6	1.5	1.7		22.6
API	6.5	2.0	1.5		
DPRT	5.9	1.4	1.7	5.6	
CDPRT	5.8	1.5	1.5	4.5	
ZnDPRT	5.4	1.5	1.4	4.0	8.1
DPHT	6.7	1.5	1.5	7.9	
CDPHT	6.5	1.5	1.5	3.3	
ZnDPHT	5.7	1.6	1.3	3.1	7.7
PRT	9.1	1.7	1.1		
CPRT	10.5	2.1	1.3		
ZnPRT	9.0	2.0	1.2		8.9

[a] Previous work reported in ref 19.

Table 4. Empirical Formulae of Mesoporous Materials and Catalysts and Some of the Ligands Used in Their Syntheses

sample	empirical formula[a]
propylamine	C_3H_9N [c]
N-(propylamino)tropone	$C_{10}H_{13}NO$ [c]
N-propyl-2-(propylamino)troponimine	$C_{13}H_{20}N_2$ [c]
N-propyl-2-(phenylamino)troponimine	$C_{19}H_{16}N_2$ [c]
API	$C_{5.2}H_{18.4}N_{1.0}Si_{14.3}O_{28.6}$
DPRT	$C_{4.0}H_{11.5}F_{2.4}NSi_{11.6}O_{23.3}$
CDPRT	$C_{4.4}H_{13.7}F_{2.2}N_{1.0}Si_{13.2}O_{26.4}$
ZnDPRT	$C_{4.6}H_{15.2}F_{2.2}NSi_{6.2}O_{12.5}Zn_{0.6}$
ZnDPRT [b]	$C_{3.8}H_{11.7}F_{1.7}NSi_{5.1}O_{10.2}Zn_{1.6}$
DPHT	$C_{5.1}H_{10.5}F_{3.8}NSi_{12.6}O_{25.2}$
CDPHT	$C_{5.1}H_{13.6}F_{1.6}NSi_{13.7}O_{27.3}$
ZnDPHT	$C_{5.1}H_{17.1}F_{1.7}NSi_{8.4}O_{16.7}Zn_{0.7}$
PRT	$C_{9.8}H_{22.3}NSi_{19.0}O_{38.0}$
CPRT	$C_{9.4}H_{22.0}NSi_{15.4}O_{30.9}$
ZnPRT	$C_{9.0}H_{24.0}N_{1.0}Si_{15.9}O_{31.7}Zn_{1.6}$

[a] Determined via elemental analysis data. [b] From previous work reported in ref 19. [c] Determined by molecular structure.

The C, H, N, F, and Zn elemental analyses for the Zn-ATI and Zn-ATO catalysts and their precursors are compiled in Table 3. For purposes of comparison, the data from the first DPRT catalyst, discussed in ref 19, is also included. As seen, the previous CAPI (methyl-capped API) material had 8.9 and 2.3 wt % C and H, respectively. Upon formation of the DPRT ligand, one would expect a marked increase the wt % C as well as noticeable increase in wt % H. An opposite trend is noticed, however, due to the substantial loss of trimethylsilyl (TMS) capping agents because of fluorination of the surface which resulted in lowered wt % C and H of 7.1 and 1.7%, corresponding to relative losses of 19.5% and 28.3% C and H content, respectively, despite the addition of ligand which was clearly evident because of color change of the powder and multiple analytical methods which have also been used in this study. The wt % F for some representative samples such as DPRT or DPHT were also included in Table 3. The elemental analyses performed on the new Zn-ATI/Zn-ATO catalysts as well as their precursors and more careful attention to compositional changes at every step of synthesis gives valuable insight to how HMDS capping after ligand synthesis improves the understanding of the CHN wt % data and how the chelation of Zn is enhanced. To better understand the chemical compositions of these new materials and how they compare to the previously synthesized ZnDPRT[19] and homogeneous equivalents of the metal-free ligands, the empirical formulas were determined for comparison (Table 4).

In the present study APTMS grafted in isopropanol to calcined SBA-15 (API) resulted in a material with 6.5, 2.0, and 1.4 wt % C, H, and N, respectively. In the case of the ATI ligands the results are somewhat deceiving. In the case of DPRT, relative losses of C and H content in comparison of the API material were found to be 10.0% C and 27.2% H. ^{29}Si CP-MAS NMR shows that T^2 silicate species, containing uncondensed silanol(−OH) groups during APTMS grafting as well as Q^2 and Q^3 are significantly reduced because of nucleophilic substitution by fluorine. The ^{13}C CP-MAS NMR shows the existence of ethoxy and isopropxy species in API, which are almost completely removed upon formation of DPRT, also because of fluorination. These substitutions result in a substantial loss of C and H, which leads to uncertainty about the quantity of DPRT loading. However, unlike the DPRT material from ref 19, the new DPRT does exhibit a slight gain in N wt % from 1.5 to 1.7 wt %. DPHT shows similar results to DPRT, with fluorination taking place with resultant loss of C and H sources; however, increases of C and N wt % are observed. This increase, in spite of fluorination, may be due to more efficient aminolysis during ATI formation, which is indicated by the ^{13}C CP-MAS NMR spectra of DPHT by comparison of the intensity of the region constituting the tropone ring to that of DPRT. If we assume that both ATI ligand syntheses occur with relatively similar reaction efficiencies, then it may also be due, in part, to the higher molecular weight of the DPHT ligand.

Supporting Information, Figures S5−S7 display the FTIR spectra of ZnDPRT, ZnDPHT, and ZnPRT as well as their synthetic precursors. The major absorptions and their corresponding chemical sources are compiled in Supporting Information, Tables S1−S3. The principal precursor of Zn-ATI and/Zn-ATO catalysts, API, (Supporting Information, Figures S5−S7 A) exhibits major absorptions at 3366, 1052, 946, and 788 cm^{-1} corresponding to Si−OH stretching, Si−O−Si stretching, and Si−O−Si bending modes indicative of the parent SBA-15. Grafting of 3-aminopropyl groups on the mesoporous material is evidenced by sp^3 hybridized C−H stretching modes at 2975 and 2930 cm^{-1}, C−N stretching at 1375 cm^{-1}, and N−H and N^+−H δ vibrational modes at 1627 and 1459 cm^{-1}, respectively, in good agreement with previously reported literature.[41,42]

It may quickly be noticed that the FTIR spectra of the Zn-ATI catalysts, that is, ZnDPRT and ZnDPHT, as well as their precursors, contain very structurally similar materials. The catalyst ZnPRT and its corresponding precursors, however, have very distinctive FTIR spectra. This is not only due to the structural similarities of the conjugated amine/imine DPHT and DPRT zinc chelates as opposed to that of the conjugated amine/carbonyl PRT chelate. Elemental analyses prove that the

dx.doi.org/10.1021/cs2000945 |ACS Catal. 2011, 1, 736–750

nucleophilic substitution of tropolone *p*-toluenesulfonate with API, a 1° amine source, which produces PRT results in higher organic loading (wt %) in the formation of the ATI materials, where activation with Et_3OBF_4 forming a corresponding vinylgous ether then undergoes aminolysis with surface aminopropyl groups to form the corresponding product. Additionally the resulting fluorinated silicate mesostructures of the Zn-ATI complexes yields structural differences such as deformation of the Si−OH stretching region (3000−3500 cm^{-1}), which splits from one major Si−OH stretch to two separate absorptions centered around 3180 and 3360 cm^{-1}, corresponding to N−H and Si−OH stretching modes, respectively, which is not shown in the case of ZnPRT. Also, the presence of silicon oxyfluoride species, as indicated by the formation of the adsorption at 720 cm^{-1} in the DPRT (Supporting Information, Figure S5 B) and DPHT (Supporting Information, Figure S6 B) samples may be seen. These changes, however, are not noticed in the case of ZnPRT (Supporting Information, Figure S7 B). HMDS capping is clearly evidenced by the presence of $Si-(CH_3)_3$ γ vibrational modes at 845 and 757 cm^{-1} in the CPRT and ZnPRT catalysts (Supporting Information, Figures S7 C and D). These peaks are not clearly seen in the case of the Zn-ATI catalysts and precursors (Supporting Information, Figures S5 and S6 C and D) presumably because of the limited surface silanols content after fluorination in the previous synthetic step. Solid-state ^{13}C NMR studies, discussed previously, also showed that the ZnPRT and its synthetic precursors have quantitative amounts of ethoxy species which are not present in the Zn-ATI samples. These groups are not present in the Zn-ATI catalysts because of either the nucleophilic substitution of alkoxy species or the substitution of surface silanols which eliminates the possibility of esterfication taking in future reactions where alcoholic solvent systems are utilized. These properties may be the reason the region of 2800−3000 cm^{-1}, corresponding to aliphatic C−H stretching modes, is significantly different for the ZnDPRT and ZnDPHT ligand series as compared that of the ZnPRT series. It may easily be noticed that the ZnPRT catalyst series has many more intense and distinct absorbances in the aliphatic C−H stretching region than that of the Zn-ATI materials.

The 1350−1650 cm^{-1} region also displayed many major absorbances that are distinct to each of the respective ligand series, and which were not present in the spectrum of the precursor API. In the case of the ZnDPRT catalyst series (Supporting Information, Figure S5 and Table S1) major absorbances are seen at approximately 1515, 1460, and 1400 cm^{-1} corresponding to C═C stretching modes from the tropone ring. The ZnDPHT catalyst series (Supporting Information, Figure S6 and Table S2) displays similar absorbances at approximately 1512 and 1465 cm^{-1} as the ZnDPRT materials. Additionally, peaks at approximately 1445, 1430, and 1411 cm^{-1} are seen, possibly due to the phenyl arm of the DPHT chelate. It may quickly be observed that the ZnPRT catalyst series (Supporting Information, Figure S7 and Table S3) is very different from the Zn-ATI materials. Unlike the latter, ZnPRT contains an absorbance at approximately 1600 cm^{-1}, corresponding to a carbonyl (C═O) stretching mode. Additionally, the only other prominent absorbances are at 1448 and 1515 cm^{-1}. While these are similar to those exhibited by the ZnATI materials, they are a much more discernible in the ZnPRT catalyst series.

The samples were further characterized by X-ray photoelectron spectroscopy (XPS). A carbon contamination peak with binding energy of 284.8 eV was chosen as a reference to compensate binding energy of the charging species. Supporting Information, Figures S8 and S9 display the XPS spectra of API, the Zn-ATI/Zn-ATO complexes, and their precursors. Specific binding energies (B.E.) (in eV) of molecular components and their respective atomic percentages (at %) are compiled in Table 5. As shown, the parent API material exhibits a N 1s binding energy of 399.0 eV. Upon formation of the ATI ligands this peaks shifts to 401.3 eV for the ATI ligands of both DPRT (Figure 8A) and DPHT (Figure 8B), and to 399.9 eV for the ATO ligand PRT (Figure 8C).

Table 5. Combined Compositional Data from XPS Spectra

sample	B.E.(eV)	area	at %
	API		
C 1s	284.8	811.4	26.6
O 1s	531.5	4362.8	48.8
Si 2p	102.2	570.9	22.9
N 1s	399.0	91.0	1.7
	DPRT		
C 1s	284.8	282.6	10.6
O 1s	531.9	3943.9	50.4
Si 2p	102.7	576.4	26.4
N 1s	401.3	95.9	2.0
F 1s	685.6	1262.6	10.7
	ZnDPRT		
C 1s	284.8	295.5	14.6
O 1s	532.5	3098.5	52.2
Si 2p	103.2	325.8	19.7
N 1s	400.3	68.2	1.9
F 1s	685.7	581.5	6.5
Zn 2p	1022.3	2986.5	5.1
	DPHT		
C 1s	284.8	335.6	14.2
O 1s	532.4	3425.4	49.6
Si 2p	103.1	488.5	25.3
N 1s	401.3	85.8	2.0
F 1s	686.5	927.0	8.9
	ZnDPHT		
C 1s	284.8	225.5	18.4
O 1s	532.0	1832.6	51.3
Si 2p	102.8	198.9	20.0
N 1s	400.2	40.7	1.9
F 1s	685.7	172.1	3.2
Zn 2p	1021.9	1821.8	5.2
	PRT		
C 1s	284.8	525.4	20.3
O 1s	532.3	4006.0	52.8
Si 2p	103.0	536.4	25.3
N 1s	399.9	75.1	1.6
	ZnPRT		
C 1s	284.8	413.9	21.0
O 1s	532.3	2899.3	50.2
Si 2p	103.0	365.5	22.7
N 1s	399.8	53.9	1.5
Zn 2p	1021.6	2587.8	4.6

dx.doi.org/10.1021/cs2000945 |*ACS Catal.* 2011, 1, 736–750

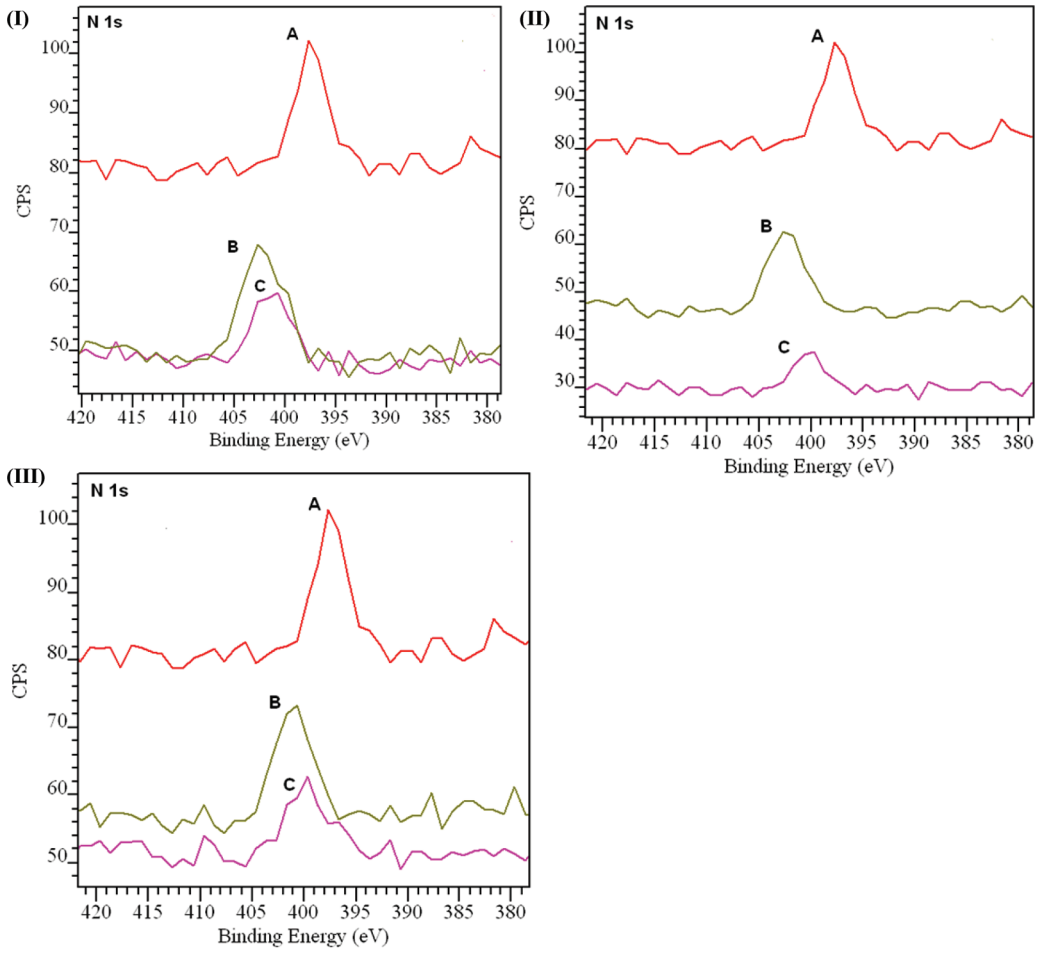

Figure 8. (I) N 1s XPS spectra of ZnDPRT series: (A) API, (B) DPRT, and (C) ZnDPRT. (II) N 1s XPS spectra of ZnDPHT series: (A) API, (B) DPHT, and (C) ZnDPHT. (III) N 1s XPS spectra of ZnPRT series: (A) API, (B) PRT, and (C) ZnPRT.

From these data it is observed that shifts toward higher B.E. occur as primary amines are converted to secondary amine or imine species. Upon $ZnMe_2$ addition, the N 1s emissions are shifted uniformly to slightly lower B.E.'s to 400.3 and 400.2 eV for the ATI ligands DPRT and DPHT, respectively, and to 399.8 eV for the ATO ligand PRT. The presence of F 1s peaks, due to the formation of silicon oxyfluoride species, are noticed in the DPRT and DPHT samples at 685.6 and 686.5 eV, respectively consistent with fluorination studies using Et_3OBF_4 as a fluorinating agent of mesoporous silica.[33] The peaks shift slightly to lower B.E.'s upon $ZnMe_2$ addition to 685.7 eV for ZnDPHT possibly due to Zn−O formation on the pore walls, resulting in polarization of the lattice. This shift may also be due to the capping of excess acidic surface silanols that may interact with adjacent fluorosilicate species. This is also evidenced by the Si 2p data. API exhibits a Si 2p B.E. of 102.2 eV. Upon post modification forming the ATI/ATO ligands, a shift to ∼103 eV is noticed with all three ligands. This trend may be due to the presence of less ionic 3-aminopropyl species covalently attached onto the surface of the substrate and reducing the emission from fully condensed silicate species within the pore walls or previously on the surface.

The Zn 2p emission spectra are shown in Figure 9, which indicate a B.E. of ∼1022 eV for all the samples, that is, ZnDPRT, ZnDPHT, and ZnPRT. Previous work performed by Futsuhara et al.[43] showed that species such as Zn_3N_2 and pure ZnO displayed Zn $2p_{3/2}$ emissions at 1022.0 and 1021.8 eV, respectively. Further work by Fu et al.[44] found ZnO to have a Zn $2p_{3/2}$ emission at 1021.1 eV and that formation of ZnO−SiO_2, or Zn−O−Si, species resulted in a shift to 1023.0 eV. Our previous studies show that Zn−O bonds formed in pure SBA-15 (Zn-SBA-15) and aminopropyl-functionalized SBA-15 (Zn-CAPI) via treatment with a solution of $ZnMe_2$ exhibited distinct binding energies of 1022.4 and 1022.7 eV, respectively.[19] Other studies have shown that ligands chelating through N, O, or S groups exhibit Zn $2p_{3/2}$ emissions ranging from 1019.3−1022.6 eV in good agreement with the Zn-ATI/Zn-ATO catalysts.[45−48]

The SBA-15 support material used for Zn-ATI and Zn-ATO catalytic sites is known to have corrugated and microporous wall structure.[49,50] Hence, we have attempted to determine whether and if the surface roughness of the SBA-15 support can influence the distribution of immobilized Zn aminotroponiminates (Zn-ATI) and Zn aminotroponates (Zn-ATO) although to the best of our knowledge probing the distribution of supported organometallic complexes such as Zn-ATI or Zn-ATO on mesoporous silicas directly is rather difficult. The approach we used involved the successful method we recently reported that enabled us to determine the distribution of supported organoamine groups on mesoporous MCM-41 material.[51] Because we used supported organoamines to subsequently attach the Zn-ATI and Zn-ATO complexes, this approach should be reasonable

dx.doi.org/10.1021/cs2000945 |*ACS Catal.* 2011, 1, 736–750

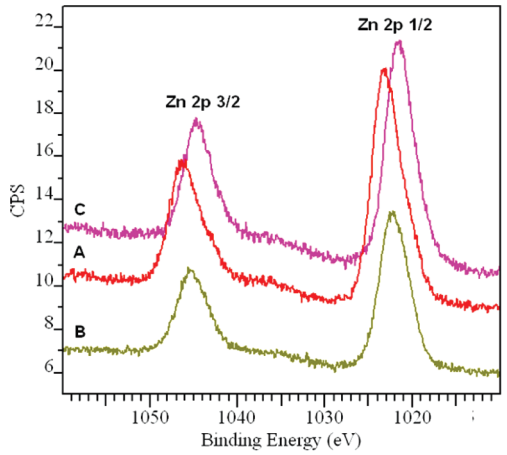

Figure 9. Zn 2p XPS spectra of (A) ZnDPRT, (B) ZnDPHT, and (C) ZnPRT.

enough to provide some information about the possible distribution of Zn-ATI and Zn-ATO complexes on the walls of SBA-15 materials.

Hence, we first synthesized SBA-15 mesostructured material, and from which we prepared calcined and solvent-extracted SBA-15, that were labeled as SBA-15-Cal and SBA-15-Ext, respectively. Solvent-extracted SBA-15 generally has a rougher surface compared to its calcined counterpart which has more annealed and smoother surface and hence, the former was used as a reference material in the study. The resulting mesoporous silica materials were functionalized with 3-aminopropyltriethoxysilane (APTMS) in isopropanol to produce aminopropyl-functionalized mesoporous silicas, that were denoted as API-SBA-15-Cal and API-SBA-15-Ext, respectively (Supporting Information, Figure S10). The distribution of the organoamine groups in the two materials were then probed with a copper test, as we reported previously.[51] The result is included in Supporting Information, Figure S11. The result indicated that the λ_{max} of the Cu^{2+}-organoamine complexes in API-SBA-15-Ext was slightly more blue-shifted compared to those in the corresponding samples made from API-SBA-15-Cal. This indicated that the organoamines in API-SBA-15-Ext were slightly more aggregated (or densely distributed) compared to those in API-SBA-15-Cal. This in turn indirectly implied that the Zn-ATI and Zn-ATO complexes in the API-SBA-15-Ext could be slightly more densely distributed compared to the ones in the API-SBA-15-Cal. The reason for the differences, however, is not necessarily the differences in the degree of corrugation (or surface roughness) between the two materials. It could also be the differences in the surface density of silanol groups, which is typically higher in solvent-extracted materials than corresponding calcined materials, which in turn affect the density of possibly grafted organoamine groups in the mesoporous silica materials.

To fully obtain more insightful information of the effect of the surface of the materials, the results were compared with those of MCM-41 based materials that are known to have smoother surface than SBA-15 based materials. The λ_{max} for organoamine-functionalized solvent-extracted MCM-41 material (API-SBA-15-Ext) showed significantly red-shifted UV−vis absorption.[51] This indicated that the organoamines in API-MCM-41-Ext were slightly more spatially distributed than those in API-Ext-SBA-15 (or the organoamines in API-SBA-15-Ext were more densely distributed than those in API-MCM-41-Ext). This, in turn, implies that supported organometallics could be more closely spaced in the former than in the latter. In this case, these differences could necessarily be due to the differences in the degree of corrugated structures between the two materials, with the more corrugated surface of SBA-15 resulting in more densely spaced supported catalysts compared to that rather smooth surface of MCM-41. Hence, it can be concluded that a difference in surface corrugation could affect the degree of distribution supported organic groups and organometallic complexes such as Zn-ATI and Zn-ATO.

Intramolecular Hydroamination Catalysis. To test the catalytic activity of the synthesized Zn-ATI/Zn-ATO catalysts for use in the intramolecular hydroamination of nonactivated alkenes, molecules with varied steric and electronic properties were synthesized. To determine the effect of how bulky (phenyl) and nonbulky (methyl) geminal substituents located β to the secondary amine altered cyclization efficiency by changing the bite angle of the quaternary carbon (i.e., Thorpe−Ingold effect), corresponding nonactivated alkenes were synthesized, having different *p*-substituted benzylic side arms of the nonactivated alkenic cyclizing agents with electron donating (−OH), electron withdrawing (-NO_2), and neutral (-H) moieties. The results from the intramolecular hydroamination catalytic trials using ZnDPRT, ZnDPHT, and ZnPRT are compiled in Table 6. Reactions were performed at 110 °C under atmospheric conditions with fast stirring. The 2,2-diphenyl substituted moieties cyclized in faster reaction times than that of the 2,2-dimethyl analogues (8 vs 12 h) and also resulted in higher overall product conversion. Prolonged reaction times for the less bulky dimethyl analogues have also been observed in many previous studies, because of the decreased bite angle resulting in a lowered reaction rate.[22,30,31] The bite angle may be altered causing changes in the distance between secondary amine and olefinic carbon, or their relative proximity, that facilitates or hinders the formation of the corresponding heterocycle. In general, it is observed that the dimethyl-substituted substrates with electron donating *p*-substituted (−OH) benzylic side arms cyclize faster than that of the relatively electroneutral benzyl (-H) species and the electron withdrawing *p*-substituted (NO_2) species, which exhibit lowered conversions over the same reaction time or lowered turn over frequencies (TOFs). For the diphenyl-substituted substrates, those containing electron donating (−OH) benzylic and electroneutral *p*-substituted benzylic side arms cyclize faster than the ones containing electron withdrawing (NO_2) species.

In addition, the following observation can be made by comparing the catalytic TOF values of the three catalysts compiled in Table 6. For cyclizing substrates containing diphenyl groups at β-position with respect to the amine, the catalytic activity of ZnDPHT was higher than that of ZnDPRT, and the catalytic activity of ZnDPRT was higher than that of ZnPRT, regardless of whether an electron donating or withdrawing *p*-substituted group was used on the benzylic side arm of the substrate (Scheme 1). For the cyclizing substrates containing dimethyl groups at β-position with respect to the amine and an electron donating group on the benzylic side arm of the substrate, the catalytic activity of ZnDPHT was again slightly higher compared to both ZnDPRT and ZnPRT. However, for the other cyclizing substrates with dimethyl groups at β-position with respect to the amine and electroneutral (H) or electron withdrawing (NO_2) groups, the catalytic efficiencies of all the three catalysts were somewhat similar, and no strong correlations were observed based on TOF values (Table 6). These results clearly show the effects of changing the types of catalysts as well as substituents of

Table 6. Comparative Data of ZnATI/ATO Catalytic Efficiency in the Intramolecular Hydroamination of Various Non-Activated Alkenes[a]

cyclizing agent	ZnDPRT (conv. %)[d]	ZnDPRT (TOF, h^{-1})[e]	ZnDPHT (conv. %)[d]	ZnDPHT (TOF, h^{-1})[e]	ZnPRT (conv. %)[d]	ZnPRT (TOF, h^{-1})[e]
R = Ph[b]						
R′ = −OH	87	0.65	86	0.68	91	0.63
R′ = −H	90	0.68	93	0.74	91	0.63
R′ = $-NO_2$	80	0.60	80	0.64	74	0.51
R = Me[c]						
R′ = −OH	75	0.38	81	0.43	81	0.37
R′ = −H	72	0.36	63	0.33	67	0.31
R′ = $-NO_2$	71	0.36	59	0.31	75	0.34

[a] Catalyst = 20 mg; Solvent = 5 mL of toluene; Cyclizing substrate = 0.15 mmol and *N,N*-dimethylanilinium tetra(pentafluorophenyl)borate = 20 mg, 0.024 mmol; Temperature = 120 °C and stirred until completion. Products were isolated via column chromatography. [b] t = 8 h. [c] t = 12 h. [d] Determined via ^{1}H NMR. [e] Calculated based on the mol product per mol catalyst per unit time. The mmol of catalyst was calculated from elemental analysis (Table 3), i.e. ZnDPRT = 0.0248 mmol Zn, ZnDPHT = 0.0236 mmol, and ZnPRT = 0.0272 mmol per gram of Zn-ATI or Zn-ATO material.

the substrate in the hydroamination reactions catalyzed by Zn-ATI- and Zn-ATO, even though the effects are only moderate in some cases. These differences can be hypothetically attributed to the favorable (or unfavorable) electronic and steric effects caused by the substituents on the reaction intermediates as well as catalysts. Further work is required to fully understand these in more detail.

4. CONCLUSIONS

In this work we expanded previous studies,[19] by synthesizing two new functionalized SBA-15 containing Zn aminotroponiminate (Zn-ATI) and Zn aminotroponato (Zn-ATO) catalytic groups. These include [*N*-propyl-2-(phenylamino)troponiminato] zinc methyl (ZnDPHT) and [2-(propylamino)troponato] zinc methyl (ZnPRT). The catalysts were characterized by various structural (small angle XRD and N_2 gas sorption) and compositional (solid-state NMR, XPS, FTIR, thermogravimetric, and elemental analyses) techniques. In general, it is observed that the catalytic properties of Zn-ATI differ from that of ZnPRT in the hydroamination of various nonactivated alkenes with varied steric and electronic properties. Moreover, investigation of the catalytic properties of the materials in hydroamination revealed that decreased bite angles (Thorpe−Ingold effect) and increased electron donation of the *p*-substituted benzylic side arm result in increased conversion efficiencies. Overall the 2,2-diphenyl cyclizing agents formed their corresponding N-containing 5-membered heterocycles at 74−94% conversion in 8 h under reflux conditions while the 2,2-dimethyl species exhibited 59−81% conversion of 12 h. The findings from this work have provided further insightful information regarding the best approaches to produce Zn-ATI and Zn-ATO based heterogeneous catalysts for the hydroamination reactions of various substrates.

■ ASSOCIATED CONTENT

Supporting Information. Thermogravimetric traces, XPS spectra, FTIR-spectra, UV−vis spectra, N_2 gas adsorption isotherms, BJH pore size distribution, and ^{1}H NMR spectra. This material is available free of charge via the Internet at http://pubs.acs.org.

■ AUTHOR INFORMATION

Corresponding Author

*Phone: (732) 445-2970. Fax: (732) 445-5312. E-mail: tasefa@rci.rutgers.edu.

Funding Sources

We gratefully acknowledge the financial assistance by the U.S. National Science Foundation (NSF), CAREER Grant CHE-1004218 and NSF DMR-0968937 for this work.

■ ACKNOWLEDGMENT

T.A. thanks the U.S. National Science Foundation (NSF) for nominating him as one of its ten NSF American Competitiveness and Innovation (NSF-ACI) Fellows for 2010 and the accompanying grant for his group's research work. We thank Dr. Sylvie Rangan for her help with XPS analysis.

■ REFERENCES

(1) Roesky, P. W.; Müller, T. E. *Angew. Chem., Int. Ed.* **2003**, *42*, 2708–2710.
(2) Pohlki, F.; Doye, S. *Chem. Soc. Rev.* **2003**, *32*, 104–114.
(3) Nobis, M.; Driessen-Hölscher, B. *Angew. Chem., Int. Ed.* **2001**, *40*, 3983–3985.
(4) Müller, T. E.; Beller, M. *Chem. Rev.* **1998**, *98*, 675–703.
(5) Hartung, C. G.; Breindl, C.; Tillack, A.; Beller, M. *Tetrahedron* **2000**, *56*, 5157–5162.
(6) Schlummer, B.; Hartwig, J. F. *Org. Lett.* **2002**, *4*, 1471–1474.
(7) Ackermann, L.; Bergman, R. G.; Loy, R. N. *J. Am. Chem. Soc.* **2003**, *125*, 11956–11963.
(8) Tillack, A.; Castro, I. G.; Hartung, C. G.; Beller, M. *Angew. Chem., Int. Ed.* **2002**, *41*, 2541–2543.
(9) Utsunomiya, M.; Kuwano, R.; Kawatsura, M.; Hartwig, J. F. *J. Am. Chem. Soc.* **2003**, *125*, 5608–5609.
(10) Shimada, T.; Yamamoto, Y. *J. Am. Chem. Soc.* **2002**, *124*, 12670–12671.
(11) Fadini, L.; Togni, A. *Chem. Commun.* **2003**, 30–31.
(12) Pawlas, J.; Nakao, Y.; Kawatsura, M.; Hartwig, J. F. *J. Am. Chem. Soc.* **2002**, *124*, 3669–3679.
(13) Pissarek, J.-W.; Schlesiger, D.; Roesky, P. W.; Blechert, S. *Adv. Synth. Catal.* **2009**, *351*, 2081–2085.
(14) Dochnahl, M.; Lçhnwitz, K.; Pissarek, J.-W.; Biyikal, M.; Schulz, S. R.; Schçn, S.; Meyer, N.; Roesky, P. W.; Blechert, S. *Chem.—Eur. J.* **2007**, *13*, 6654–6666.
(15) Meyer, N.; Lçhnwitz, K.; Zulys, A.; Roesky, P. W.; Dochnahl, M.; Blechert, S. *Organometallics* **2006**, *25*, 3730–3734.
(16) Zulys, A.; Dochnahl, M.; Hollmann, D.; Lçhnwitz, K.; Herrmann, J.-S.; Roesky, P. W.; Blechert, S. *Angew. Chem., Int. Ed.* **2005**, *44*, 7794–7798.
(17) Biyikal, M.; Porta, M.; Roesky, P. W.; Blechert, S. *Adv. Synth. Catal.* **2010**, *352*, 1870–875.

(18) Dochnahl, M.; Lohnwitz, K.; Luhl, A.; Pissarek, J.-W.; Biyikal, M.; Roesky, P. W.; Blechert, S. *Organometallics* **2010**, *29*, 2637–2645.
(19) Duncan, C. T.; Flitsch, S.; Asefa, T. *ChemCatChem* **2009**, *1*, 365–368.
(20) Liu, Z.; Hartwig, J. F. *J. Am. Chem. Soc.* **2008**, *130*, 1570–1571.
(21) Bender, C. F.; Widenhoefer, R. A. *J. Am. Chem. Soc.* **2005**, *127*, 1070–1071.
(22) Majumder, S.; Odom, A. L. *Organometallics* **2008**, *27*, 1174–1177.
(23) Kim, Y. K.; Livinghouse, T.; Horino, Y. *J. Am. Chem. Soc.* **2003**, *125*, 9560–9561.
(24) Hong, S.; Marks, T. J. *Acc. Chem. Res.* **2004**, *37*, 673–686.
(25) Penzien, J.; Müller, T. E.; Lercher, J. A. *Microporous Mesoporous Mater.* **2001**, *48*, 285–291.
(26) Muller, T. E.; Lercher, J. A.; Nhu, N. V. *AIChE J.* **2003**, *49*, 214–224.
(27) Penzien, J.; Haessner, C.; Jentys, A.; Köhler, K.; Müller, T. E.; Lercher., J. A. *J. Catal.* **2004**, *221*, 302–312.
(28) Penzien, J.; Müller, T. E.; Lercher, J. A. *Chem. Commun.* **2000**, 1753–1754.
(29) Dochnahl, M.; Löhnwitz, K.; Pissarek, J.-W.; Roesky, P. W.; Blechert, S. *Dalton Trans.* **2008**, 2844–2848.
(30) Dochnahl, M.; Pissarek, J.-W.; Blechert, S.; Löhnwitz, K.; Roesky, P. W. *Chem. Commun.* **2006**, 3405–3407.
(31) Zulys, A.; Dochnahl, M.; Hollmann, D.; Löhnwitz, K.; Herrmann, J.-S.; Roesky, P. W.; Blechert, S. *Angew. Chem., Int. Ed.* **2005**, *44*, 7794–7798.
(32) Herrmann, J.-S.; Luinstra, G. A.; Roesky, P. W. *J. Organomet. Chem.* **2004**, *689*, 2720–2725.
(33) Duncan, C. T.; Biradar, A. V.; Rangan, S.; Mishler, R. E.; Asefa, T. *Chem. Mater.* **2010**, *22*, 4950–4963.
(34) Dias, H. V. R.; Jin, W.; Ratcliff, R. E. *Inorg. Chem.* **1995**, *34*, 6100–6105.
(35) Doering, W. v. E.; Hiskey, C. F. *J. Am. Chem. Soc.* **1952**, *74*, 5688–5693.
(36) Claramunt, R. M.; Sanz, D.; Pérez-Torralba, M.; Pinilla, E.; Torres, M. R.; Elguero, J. *Eur. J. Org. Chem.* **2004**, 4452–4466.
(37) Sharma, K. K.; Buckley, R. P.; Asefa, T. *Langmuir* **2008**, *24*, 14306–14320.
(38) Sharma, K. K.; Asefa, T. *Angew. Chem., Int. Ed.* **2007**, *46*, 2879–2882.
(39) Xie, Y.; Sharma, K. K.; Anan, A.; Wang, G.; Biradar, A. V.; Asefa, T. *J. Catal.* **2009**, *265*, 131–140.
(40) Suzuki, T. M.; Nakamura, T.; Fukumoto, K.; Yamamoto, M.; Akimoto, Y.; Yano, K. *J. Mol. Catal. A: Chem.* **2008**, *280*, 224–232.
(41) Chong, A. S. M.; Zhao, X. S. *J. Phys. Chem. B* **2003**, *107*, 12650–12657.
(42) Luan, Z.; Fournier, J. A.; Wooten, J. B.; Miser., D. E. *Microporous Mesoporous Mater.* **2005**, *83*, 150–158.
(43) Futsuhara, M.; Yoshioka, K.; Takai, O. *Thin Solid Films* **1998**, *322*, 274–281.
(44) Fu, Z.; Yang, B.; Li, L.; Dong, W.; Jia, C.; Wu, W. *J. Phys.: Condens. Matter.* **2003**, *15*, 2867–2873.
(45) Cothern, C. R.; Moddeman, W. E.; Albridge, R. G.; Sanders, W. J.; Kelly, P. L.; Hanley, W. S.; Field, L. *Anal. Chem.* **1976**, *48*, 162–166.
(46) Thirumaran, S.; Ramalingama, K.; Bocelli, G.; Cantoni, A. *Polyhedron* **1999**, *18*, 925–930.
(47) Sirtori, V.; Zambon, F.; Lombardi, L. *J. Electron. Mater.* **2000**, *29*, 463–467.
(48) Casas, J. S.; Castaño, M. V.; García-Tasende, M. S.; Rodríguez-Castellón, E.; Sánchez, A.; Sanjuán, L. M.; Sordo, J. *Dalton Trans.* **2004**, 2019–2026.
(49) Zukal, A.; Šiklová, H.; Čejka, J. *Langmuir* **2008**, *24*, 9837–9842.
(50) Gommes, C. J.; Friedrich, H.; Wolters, M.; de Jong, P. E.; de Jongh, K. P. *Chem. Mater.* **2009**, *21*, 1311–1317.
(51) Sharma, K. K.; Anan, A.; Buckley, R. P.; Ouellette, W.; Asefa, T. *J. Am. Chem. Soc.* **2008**, *130*, 218–228.